

Sources of contrast in confocal reflectance imaging

Andrew K. Dunn, Colin Smithpeter, A. J. Welch, and Rebecca Richards-Kortum

The relationship between optical properties and image contrast in confocal imaging is investigated. A Monte Carlo simulation has been developed to analyze the effects of changes in scattering, index of refraction, and absorption in a three-layer medium. Contrast was calculated from the computed signal-to-background ratios for changes in tissue optical properties. Results show that the largest source of contrast is changes in refractive index. © 1996 Optical Society of America

1. Introduction

Three-dimensional reflectance imaging such as confocal or optical coherence tomography uses light reflected from a small localized volume of tissue to form images. In confocal imaging a pinhole aperture placed at the detector allows light from a small volume to be detected while light from outside that volume is rejected. Useful images are obtained when changes in the physiological structure of the tissue being imaged produce changes in the detected light, yielding contrast. However, the ability to differentiate between normal and abnormal tissue depends on the ability to interpret the source of reflected light within the sample. Intuitively, there are two possible sources of signal contrast in reflected-light images at the microscopic scale ($\sim 5 \mu\text{m}$): local changes in refractive index and changes in local absorption. Despite recent reports of *in vivo* confocal and optical coherence images at the cellular level,¹⁻³ the relative contributions of each of these sources to contrast are not yet well understood.

Signal contrast is the most important factor in image quality when the signal-to-noise ratio is less than ~ 5 .⁴ Above this signal-to-noise ratio, image quality is determined by the modulation transfer function of the system. Below this, however, imaging of cellular structures relies on the ratio of the detected photons originating from the sample vol-

ume to those detected photons originating from outside the sample volume. When imaging is done in turbid media, this ratio will generally be low, so an understanding of the source of contrast is important in evaluating images and in choosing the wavelength or combinations of wavelengths to maximize the contrast of the desired target.

Tissue optical properties are typically characterized by the scattering coefficient μ_s , anisotropy factor g , absorption coefficient μ_a , and refractive index n . In this paper we address the relative contributions of the refractive index, scattering coefficient, and absorption coefficient to signal contrast in a confocal geometry. To isolate the contributions of each parameter, a Monte Carlo simulation has been developed.

2. Monte Carlo Simulation

To investigate the effects of optical properties on image contrast, a Monte Carlo simulation was developed with the confocal excitation and collection geometry shown in Fig. 1. Photons from a focused, Gaussian beam were injected into the tissue by varying the starting point on the tissue surface along the x axis so that each photon had initial coordinates⁵:

$$\begin{aligned}x &= r_s[-\ln(1 - \xi)/2]^{1/2}, \\y &= 0, z = 0,\end{aligned}\quad (1)$$

where ξ is a uniformly distributed random number between 0 and 1 and r_s is the $1/e^2$ radius of the spot size of the beam on the tissue surface given by

$$r_s = \frac{D}{2} \left(1 - \frac{h}{f}\right), \quad (2)$$

The authors are with the Department of Electrical and Computer Engineering, Biomedical Engineering Program, University of Texas at Austin, Austin, Texas 78712.

Received 5 September 1995; revised manuscript received 29 January 1996.

0003-6935/96/193441-06\$10.00/0

© 1996 Optical Society of America

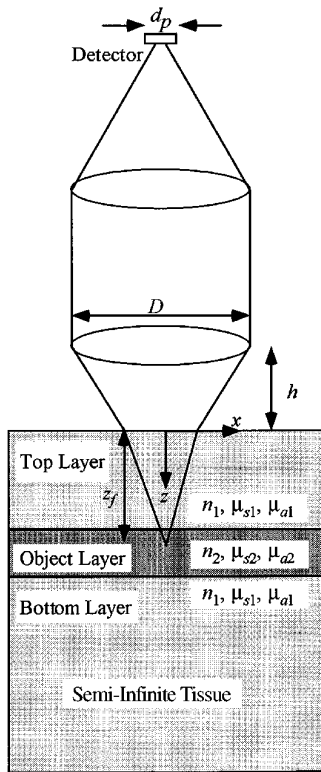


Fig. 1. Confocal geometry for the Monte Carlo simulation. The optical properties of the object layer are varied whereas the properties of the top and bottom layers are matched and constant.

where D is the diameter of the beam at the objective lens, h is the height of the lens above the surface of the tissue, and f is the focal length of the lens. The tissue was assumed to have cylindrical symmetry, and photons were launched along a radial line defined by the x axis as in Eq. (1). The initial directional cosines (μ_x, μ_y, μ_z) for each photon are a function of the starting coordinates (x, y, z):

$$\mu_x = \frac{-x}{(x^2 + z_f^2)^{1/2}}, \quad \mu_y = 0, \quad \mu_z = \frac{z_f}{(x^2 + z_f^2)^{1/2}}, \quad (3)$$

where z_f is the depth of the focal plane in the tissue and is given by

$$z_f = \left(1 - \frac{h}{f} \left[\left(\frac{D}{2} \right)^2 + f^2 \left(\frac{n_1}{n_{\text{air}}} \right)^2 - \left(\frac{D}{2} \right)^{2/2} \right] \right)^{1/2}, \quad (4)$$

where n_1 and n_{air} are the refractive indices of the tissue and the outside medium, respectively. In the case in which $n_1 = n_{\text{air}}$, Eq. (4) simplifies to $z_f = f - h$.

After the photons were launched, they were propagated according to standard Monte Carlo methods in a multilayered medium⁶ with a Henyey-Greenstein phase function used for scattering. For each photon being backscattered and returning to the top surface of the tissue, the coordinates (x_d, y_d) at which it intersected the detector plane were computed with a geometric ray trace.⁷ The photon was counted as detected if $(x_d^2 + y_d^2)^{1/2} < 0.5d_p$, where d_p is the

detector diameter. At each focal depth the total number of detected photons was divided by the total number of photons launched to determine the fraction detected.

A three-layer, semi-infinite tissue model was used to assess the individual contributions of optical properties to signal contrast by imaging a layer of tissue located between two other layers. The properties of the object layer (Fig. 1) were varied whereas the properties of the top and bottom layers were fixed. By scanning the focal plane of the confocal system through the object layer, the change in signal level between the three layers could be calculated as a measure of contrast. The resulting images of the object layer provided information about the effects of varying optical properties on signal contrast. To scan the focal plane of the confocal system through the layers, the height of the objective lens above the tissue was varied and the fraction of photons detected at each lens height was recorded.

The optical properties used in the simulations are summarized in Table 1. In all simulations the refractive index of the outside medium was assumed to be 1.0 and the anisotropy factor, g , of all tissue layers was 0.9. The anisotropy factor was not varied because, even for layered tissues, g changes little.⁸ The individual contributions to contrast were measured by changing one property of the object layer while the other properties were identical to those of the surrounding layers. The difference in refractive index between the layers was incremented in steps of 0.05 to a maximum difference of 0.4. For each increment a separate simulation was run. The scattering and absorption mismatches varied from 50 to 500 cm^{-1} .

The optical properties of the surrounding layers were chosen to be representative of soft-tissue optical properties in the near-IR region (800 nm).⁸ The absorption coefficient (1 cm^{-1}) was assumed to be much less than the scattering coefficient (100 cm^{-1}). The thickness of the object layer was 50 μm in all simulations, and its location beneath the surface was either 1, 2, or 3 optical depths (OD), where 1 OD is defined as the reciprocal of the total attenuation coefficient, μ_t :

$$\text{OD} = \frac{1}{\mu_t} = \frac{1}{\mu_s + \mu_a}. \quad (5)$$

The lens parameters used in the simulation were a diameter of 8 mm and a focal length of 10.1 mm, giving a numerical aperture of 0.4. The detector, which acted as the effective confocal pinhole, had a

Table 1. Range of Optical Properties Used in Monte Carlo Simulation

Layer	d^a	n	$\mu_s (\text{cm}^{-1})$	$\mu_a (\text{cm}^{-1})$	g
1	100–300 μm	1.3	100	1	0.9
2	50 μm	1.3–1.7	100–400	1–500	0.9
3	1 cm	1.3	100	1	0.9

^a d is the thickness of each layer.

diameter of 8 μm . This numerical aperture with a pinhole diameter of 8 μm gave the simulated confocal system an axial resolution of 16 μm (full width at half-maximum), which was calculated by simulating a mirror passing through the focal plane and recording the detected signal as a function of focal plane depth. This is in agreement with the theoretical axial resolution for the same system parameters, calculated to be 15 μm (full width at half-maximum).⁹

The signal-to-background ratio was computed from each simulation. It is defined as the ratio of the detected fraction of photons when the properties of the object layer are different from the surrounding layers to the detected fraction when the tissue is homogeneous. To compute the ratio, each simulation was divided by the background signal obtained from a homogeneous sample in which the properties of all three layers are equal. Because of the refractive-index of mismatch at the object layer, the focal-plane depth at a given lens height h differed slightly from the case of the homogeneous tissue. Therefore it was necessary to interpolate the background signal from the homogeneous tissue to find the value that matched each focal-plane depth of the mismatched sample.

3. Results

A. Refractive Index

The effects of changes in the refractive index of the object layer on the signal-to-background ratio from the three-layer sample are shown in Figs. 2 and 3. When the inhomogeneity is at 1 OD (100 μm), the mismatches in the refractive index at the front and back surfaces of the object layer are manifested as separate peaks in the signal-to-background ratio. An expanded view of the signal-to-background ratio when $\Delta n = 0.05$ ($n_2 = 1.35$) is shown in the inset in Fig. 2. Although the amplitude of the signal to background is much smaller for the $\Delta n = 0.05$ case, a

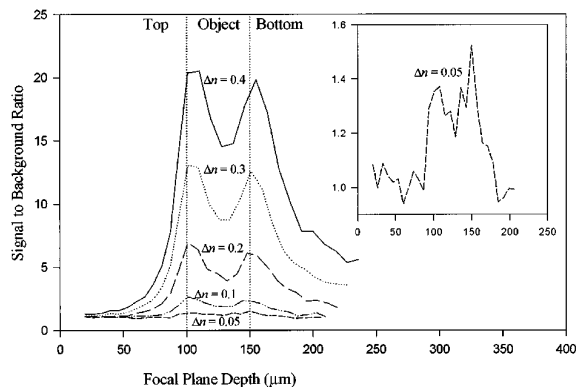


Fig. 2. Signal-to-background ratio as a function of the focal-plane depth in the tissue with the object layer located at a depth of 100 μm (1 OD) for a range of index mismatches. The value for Δn on each curve indicates the refractive-index mismatch between the object layer and the surrounding layers. Inset: expanded view of the case in which $\Delta n = 0.05$.

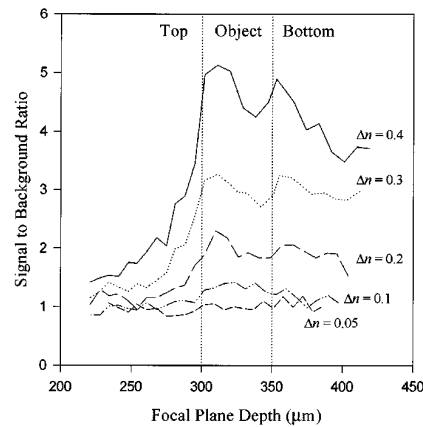


Fig. 3. Signal-to-background ratio as a function of the focal-plane depth in the tissue with the object layer located at a depth of 300 μm (3 OD) for a range of index mismatches.

change in signal can be seen at the edges of the object layer.

As the depth of the object layer increases to 3 OD (300 μm) below the surface (Fig. 3), changes in the signal-to-background ratio from the presence of the object layer are apparent for index differences as low as 0.1. At 3 OD the faces of the object layer can be observed only at large index mismatches (>0.2). Below this, although an object produces changes in the signal-to-background ratio, it is difficult to identify its front and back surfaces. Figure 3 illustrates that scattering starts to play a role as the depth of the focal plane increases in the tissue. The amplitude from the back faces of the object layer is less pronounced than that from the front face because more photons have been scattered out of the beam path and are rejected by the confocal geometry. With small changes in index, $\Delta n = 0.1$, the reflection from the back face of the object layer becomes obscured because of multiply scattered photons.

B. Scattering

The effects of different scattering coefficients of the object layer on the signal-to-background ratio at 1 OD are shown in Fig. 4. In these simulations the refractive indices were the same for all layers. A large increase in scattering results in a single peak in the signal-to-background ratio as opposed to two peaks in the case of index mismatches. The peak is observable when the change in scattering is 50 cm^{-1} ($\mu_{s,\text{obj}} = 150 \text{ cm}^{-1}$) and the top layer is at 1 OD (100 μm). Beyond the object layer the signal-to-background ratio can fall to less than one because of the increased scattering and light loss in the object layer.

The signal to background for different changes in the scattering coefficient when the object layer is located 3 OD from the surface is illustrated in Fig. 5. The object layer produces changes to varying degrees in the signal-to-background ratio, depending on the magnitude of the scattering increase between the layers. As the scattering coefficient of the object layer is increased, the number of photons detected

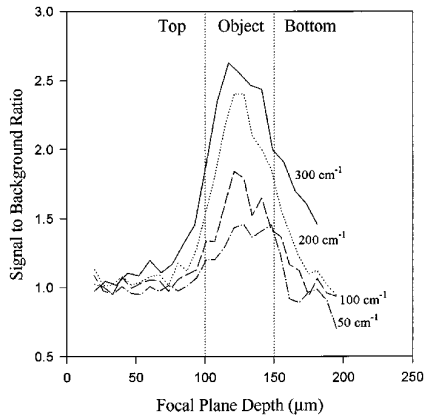


Fig. 4. Signal-to-background ratio resulting from changes in the scattering coefficient of the object layer. The mismatch in the scattering coefficient indicated on each curve is the difference in scattering between the object layer and the surrounding layers ($\mu_{s1} = 100 \text{ cm}^{-1}$). The front surface of the object layer is located at a depth of 100 μm (1 OD).

from that layer increases as demonstrated by the increase in the signal-to-background ratio.

C. Absorption

The signal-to-background ratio when the object layer has absorption properties different from the other layers and is located at 1 OD is shown in Fig. 6. When $\mu_{a2} = 200 \text{ cm}^{-1}$, there is little drop in the signal to background. At extremely high absorption ($\mu_a = 500 \text{ cm}^{-1}$) the change in signal level from the background is quite evident. The back face of the object layer cannot be distinguished for the case of absorption changes as it was for refractive-index changes because most photons reaching the boundary between the object and the bottom layer are either absorbed or scattered and subsequently rejected by the confocal geometry.

At depths greater than 2 OD, there is little change in the signal-to-background ratio from changes in absorption, even for large changes ($\Delta\mu_a = 500 \text{ cm}^{-1}$).

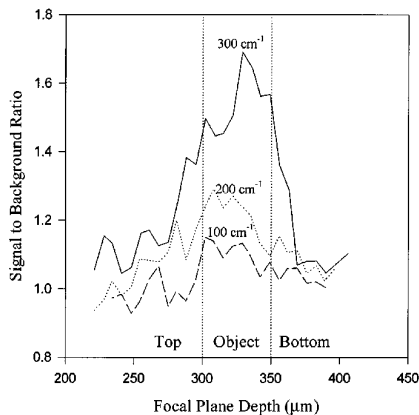


Fig. 5. Signal-to-background ratio resulting from changes in the scattering coefficient between the layers. The scattering indicated on each curve is the difference between the object layer and the surrounding layers ($\mu_{s1} = 100 \text{ cm}^{-1}$). The front surface of the object layer is located at a depth of 300 μm (3 OD).

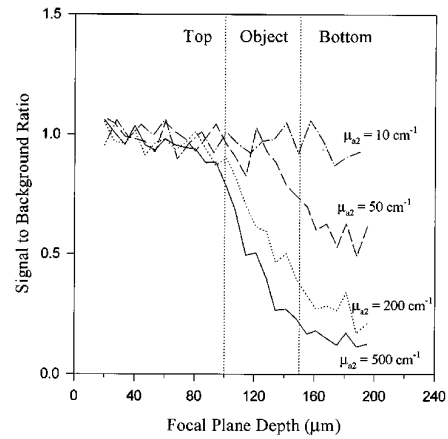


Fig. 6. Signal-to-background ratio with a highly absorbing object layer. The object layer is located at a depth of 100 μm (1 OD).

The signal-to-background ratio at 3 OD (not shown) contains little variation for all absorption values.

4. Discussion

To understand the relative contributions of tissue optical properties to contrast, we calculated a measure of contrast from the signal-to-background ratio. Contrast was defined as

$$\text{contrast} = \frac{P_s - P_b}{P_s + P_b}, \quad (6)$$

where P_s is the maximum value of the detected fraction of photons in the case in which the object layer had different optical properties than the other layers and P_b is the detected fraction of photons from the homogeneous tissue, or the background level, at the same focal plane depth as P_s . For example, P_s was located near the interface of the top and object layers in the case of index mismatches.

The contrast as a function of change in the refractive index, when the object layer is located 1, 2, and 3 OD (100, 200, 300 μm) from the tissue surface is shown in Fig. 7. As the change in index decreases,

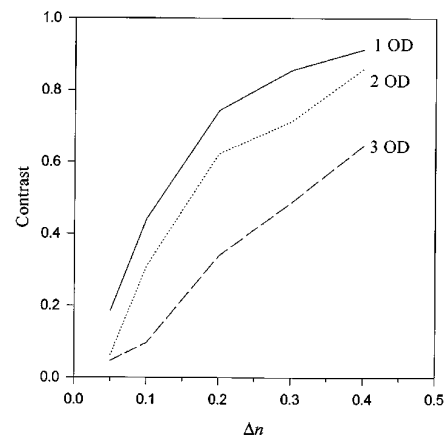


Fig. 7. Contrast as a function of the increase in refractive index, $\Delta n = n_2 - n_1$, with the object layer at three different depths [100 μm (1 OD), 200 μm (2 OD), 300 μm (3 OD)].

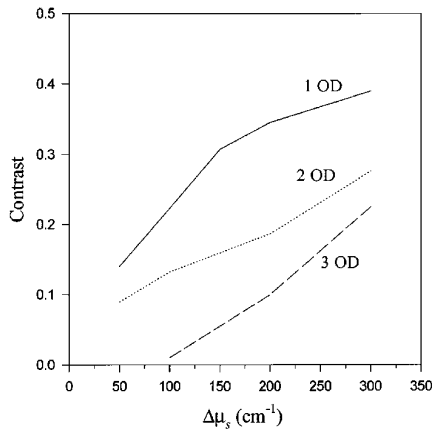


Fig. 8. Contrast as a function of change in scattering, $\Delta\mu_s = \mu_{s2} - \mu_{s1}$, with the object layer at three different depths [100 μm (1 OD), 200 μm (2 OD), 300 μm (3 OD)].

the contrast approaches zero. As expected, the largest contrast produced for a given change in refractive index occurs when the inhomogeneity is located at 1 OD. At greater depths, fewer photons reach the inhomogeneity because of multiple scattering, and some of these photons backscattered from the inhomogeneity are scattered out of the confocal path and not detected.

Equation (6) was also used to calculate the contrast produced by changes in scattering between layers. In this case the maximum signal, P_s , was located in the center of the object layer where the signal peak occurs. The contrast produced by scattering changes for depths ranging from 1 to 3 OD is illustrated in Fig. 8. As in the case of refractive-index changes, the contrast decreases with depth, and at 3 OD there is little contrast unless the changes in scattering are large ($>250 \text{ cm}^{-1}$).

The amount of contrast produced solely by scattering is significantly less than that produced by index mismatches. Scattering in tissue is typically forward directed with anisotropies, g , of 0.9 or greater. Therefore few photons are backscattered and detected, resulting in poor signal-to-noise ratios and image quality. When the object to be imaged is at a depth of 1 OD, the small fraction of photons that are backscattered can be detected because most of them exit the tissue without further scattering. As the depth of the layer or object to be imaged increases, the magnitude of the signal decreases and the noise increases. The signal decreases because more photons are scattered out of the illumination beam and do not reach the sample volume at the focal plane as the depth of the object increases. Of those that do reach the sample volume and are backscattered, many are not detected because of scattering out of the confocal geometry on the return trip, thus decreasing the actual signal. In addition, the noise level, considered to consist of background photons that are detected but originate outside the focal volume,¹⁰ increases from photons backscattered outside the sample volume in such a way as to be

detected. This leads to a reduction in both the signal-to-background ratio and contrast.

The contrast produced by changes in absorption between the layers is shown in Fig. 9. In this case the signal level, P_s , was measured at the middle of the object layer. The decrease in the contrast produced by an absorber at 1 and 2 OD is greater than the decrease between depths for changes in refractive index or scattering. This suggests that absorbers are more difficult to image at more than 1 OD with a near-IR source because absorption of tissue in the near-IR and visible region is minimal.

In Figs. 7–9 the contrast is plotted against changes in optical properties. When they are compared directly, it appears that the refractive index produces the most contrast followed by absorption and then scattering. However, we must consider the changes in optical properties encountered in actual tissues to determine the sources of contrast in *in vivo* images. In Fig. 10 the contrast produced by changes in refractive index, scattering, and absorption at 1 OD is plotted for comparison. The arrows represent the changes in each property that are likely to be found in tissue. The difference in refractive index between cellular components is the primary source of index variation in tissue. For example, the difference between the index of the extracellular fluid and the cell membrane can be as much as 0.05–0.1 (arrow labeled Cells).¹¹ In addition melanin, which has been found to be a significant source of contrast in *in vivo* confocal images,² has an index of refraction of ~ 1.7 (arrow labeled Melanin).¹² From Fig. 10 it is evident that changes in index of refraction are the largest source of contrast for the optical properties typically found in tissue, whereas absorption changes produce the least contrast because of the small changes in the absorption coefficient.⁸

In comparing the relative contributions of the scattering coefficient and refractive index, we must take the sample volume of the confocal system into consideration. The scattering coefficient repre-

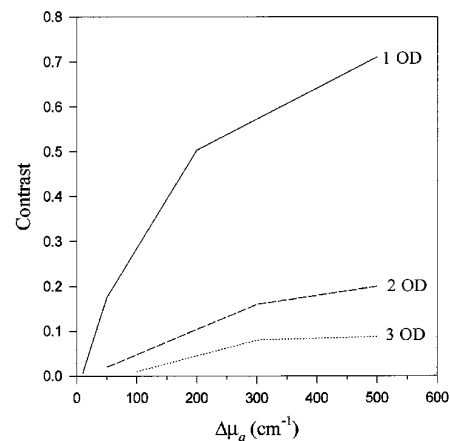


Fig. 9. Contrast as a function of change in absorption with the object layer at three different depths [100 μm (1 OD), 200 μm (2 OD), 300 μm (3 OD)].

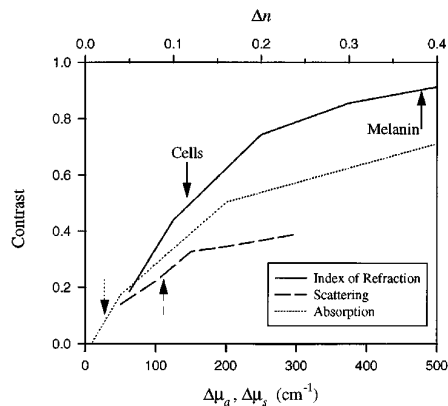


Fig. 10. Comparison of contrast produced by changes in the refractive index, scattering, and absorption at 1 OD. The arrows represent changes likely to be encountered in actual tissue.

sents an average effect of local variations in the refractive index within and around cells. For local changes in refractive index to be detected, the volume of tissue interrogated must be small. Otherwise the index variations over an area are detected. In low-resolution confocal systems¹³ that image the macroscopic structure of tissue, changes in bulk optical properties are detected. The results from this research are directly applicable to the imaging of macroscopic tissue structure. Changes in scattering are more likely to produce contrast than changes in absorption as demonstrated in Fig. 10. Microscopic changes in refractive index are not detected because the sample volume is greater than the scale of the index changes so that an average effect of the index changes is detected.

In confocal systems used for tissue imaging with lateral and axial resolution of less than $\sim 5 \mu\text{m}$, it is possible to detect the index variations between cell components.² In these systems, contrast is produced by the changes in refractive index between cell components, and only single-scatter photons are detected. Therefore changes in macroscopic scattering do not produce any contrast but serve only to limit the number of detected single-scatter photons from index changes, decreasing the contrast. Scattering and absorption of photons outside the sample volume decrease the number of photons reaching the sample volume. Similarly scattering and absorption of photons reflected from the sample volume decrease the number of photons reaching the tissue surface and being detected.

In actual tissue the cellular structures providing the changes in index have varying shapes. The amount of backscatter from a particular location, which is characterized on the macroscopic level by the scattering coefficient and anisotropy factor, depends on the magnitude of the change in the refractive index and the size and shape of the structure within the sample volume. In the simulations pre-

sented here the effects of the magnitude of the index change were investigated. Because the layers of the simulated tissue were planar, the effect of shape was not considered. Therefore these results are a first-order approximation to the signal obtained from microscopic imaging.

5. Conclusions

This research has demonstrated that the refractive-index changes in tissue are the greatest source of contrast in confocal images of the microscopic structure of tissue. Scattering degrades the signal-to-background ratio and contrast levels by reducing the number of single-scatter photons produced and detected. Absorption changes in tissue in the near-IR are not large enough to produce significant contrast at more than 1 OD.

References

1. W. Petroll, H. Cavanagh, and J. Jester, "Three-dimensional imaging of corneal cells using *in vivo* confocal microscopy," *J. Microsc.* **170**, 213–219 (1993).
2. M. Rajadhyaksha, M. Grossman, D. Esterwitz, R. Webb, and R. Anderson, "*In vivo* confocal scanning laser microscope of human skin: melanin provides strong contrast," *J. Invest. Dermatol.* **104**, 946–952 (1995).
3. J. Schmitt, A. Knuttel, M. Yadlowski, and M. Eckhaus, "Optical-coherence tomography of a dense tissue: statistics of attenuation and backscattering," *Phys. Med. Biol.* **1705–1720** (1994).
4. R. Webb and G. Hughes, "Detectors for scanning video imagers," *Appl. Opt.* **32**, 6227–6235 (1993).
5. S. Jacques and L. Wang, "Monte Carlo modelling of light transport in tissue," in *Optical-Thermal Response of Laser Irradiated Tissue*, A. Welch and M. V. Gemert, eds. (Plenum, New York, 1995), Chap. 4, pp. 1–5.
6. S. Prahl, S. Jacques, and A. Welch, "A Monte Carlo model of light propagation in tissue," in *Dosimetry of Laser Radiation in Medicine and Biology*, G. J. Mueller and D. H. Sliney, eds. (SPIE Press, Bellingham, Wash., 1989), Vol. ISO5, pp. 102–111.
7. J. Schmitt, A. Knuttel, and M. Yadlowski, "Confocal microscopy in turbid media," *J. Opt. Soc. Am. A* **11**, 2226–2235 (1994).
8. W. Cheong, S. Prahl, and A. Welch, "A review of the optical properties of biological tissue," *IEEE J. Quantum Electron.* **26**, 2166–2185 (1990).
9. T. Wilson, "The role of the pinhole in confocal imaging systems," in *Handbook of Biological Confocal Microscopy*, J. B. Pawley, ed. (Plenum, New York, 1995), Chap. 11, pp. 167–182.
10. D. Sandison and W. Webb, "Background rejection and signal-to-noise optimization in confocal and alternative fluorescence microscopes," *Appl. Opt.* **33**, 603–615 (1994).
11. J. Maier, S. Walker, S. Fantini, M. Franceschini, and E. Gratton, "Possible correlation between blood glucose concentration and the reduced scattering coefficient of tissues in the near infrared," *Opt. Lett.* **19**, 2062–2064 (1994).
12. I. Vitkin, J. Woolsey, B. Wilson, and R. Anderson, "Optical and thermal characterization of natural (*sepia officinalis*) melanin," *Photochem. Photobiol.* **59**, 455–462 (1994).
13. R. Richards-Kortum, A. Durkin, and J. Zeng, "Description and performance of a fiber-optic confocal fluorescence spectrometer," *Appl. Spectrosc.* **48**, 350–355 (1994).